Eur. Phys. J. B **8**, 371–376 (1999)

THE EUROPEAN PHYSICAL JOURNAL B

EDP Sciences

Forward Raman scattering in GaAs/AlAs superlattices: Study of optical phonon anisotropy

D.A. Tenne[1,2,a], V.A. Haisler[2], N.T. Moshegov[2], A.I. Toropov[2], A.P. Shebanin[3], and D.R.T. Zahn[1]

[1] Institut für Physik, Technische Universität Chemnitz, 09107 Chemnitz, Germany
[2] Institute of Semiconductor Physics, 630090 Novosibirsk, Russia
[3] United Institute of Geology, Geophysics and Mineralogy, 630090 Novosibirsk, Russia

Received 9 September 1998 and Received in final form 22 October 1998

Abstract. We present the forward Raman scattering study of zone-centre optical phonon anisotropy in short-period GaAs/AlAs superlattices. Experiments were performed on specially prepared superlattice structures having anti-reflection dielectric coatings and removed substrates. The experimental data are compared with the angular dispersion of superlattice optical phonons calculated within the dielectric susceptibility model. We have found a good agreement between the experimental data and the calculations taking into account interface disorder.

PACS. 63.22.+m Phonons in low-dimensional structures and small particles – 78.30.Fs III-V and II-VI semiconductors

1 Introduction

Optical phonons of GaAs/AlAs superlattices (SL's) have been the subject of many experimental and theoretical studies over the last 15 years (for a review see *e.g.* Refs. [1,2]. The basic properties of lattice vibrations are well understood, especially for SL's grown in the [001] direction. Phonons propagating along the SL axis (at zero angle Θ between the wave vector $\mathbf{q}$ and growth direction z) are confined in either GaAs or AlAs layers due to the large mass difference of Ga and Al atoms [1–3]. For off-axis propagation ($\Theta \neq 0$) the infrared-active optical phonons were predicted by different models [4–8] to exhibit significant angular dispersion. The odd-order confined optical mode frequencies strongly depend on Θ even at the centre of the Brillouin zone, *i.e.* when $|\mathbf{q}| \to 0$. This zone-center optical phonon anisotropy is due to macroscopic electric fields carried by optical phonons in SL's formed by polar semiconductors. Even-order modes do not generate long-range fields because of cancellation of the overall dipole moment. Therefore, even modes do not reveal angular dispersion for small $|\mathbf{q}|$ values [6–8].

The phonon properties of semiconductor superlattices are mainly studied experimentally by Raman spectroscopy [1,2]. Many papers reporting the Raman scattering by confined GaAs [1–3] and AlAs [9] optical phonons can be found in literature. However, most experimental studies have been performed in traditional backscattering geometry from the (001) surface. Such a geometry only allows the observation of phonons propagating along the SL axis. Experiments that directly study phonons having off-axis wave vector component are still rare, especially for AlAs phonons. These are investigations under in-plane excitation *via* a cleaved or polished edge of the SL sample using micro-Raman technique [10–12] or by exploiting a waveguide structure [13].

In the present paper we study the optical phonon anisotropy in short-period GaAs/AlAs SL's by Raman scattering in forward geometry, where the laser beam is incident along the SL axis z and scattered light is collected at a small angle with respect to z. For such a geometry the wavevector transfer is normal to the SL axis, and Raman spectra reveal features of in-plane vibrational excitations. Comparison of the forward and backscattering spectra provides the information about zone-centre optical phonon anisotropy in both GaAs and AlAs. Our data show some qualitative disagreement with the angular dispersion calculated for ideal SL with sharp interfaces. In a real superlattice interface disorder is well-known to have a strong effect on the confined optical mode frequencies [14–17]. We have determined the actual sample parameters (layer thicknesses and interface width) from Raman backscattering data of folded acoustic and confined optical phonons and then performed a calculation of the angular dispersion using the dielectric susceptibility model [8] taking into account interface disorder. In this case we have found good agreement with the experimental results.

2 Experiment

Principal difficulties of forward Raman experiments are caused by the necessity of removing the thick

[a] e-mail: tenne@thermo.isp.nsc.ru

(400–500 μm) opaque GaAs substrate without damaging the thin (0.1–0.5 μm) SL layer. Also light reflection from the SL-air interface leads to backscattering contribution in forward Raman spectra that causes difficulties in the correct interpretation of Raman spectra. To avoid these problems we have performed Raman experiments on specially prepared SL structures. Short-period $(GaAs)_m(AlAs)_m$ SL's were grown by molecular beam epitaxy on (001) GaAs substrates. The nominal layer thicknesses m are 7 and 5 monolayers, and the total numbers of periods are 100 and 150 for samples A and B, respectively. Anti-reflection dielectric coatings (quarter-wavelength ZrO_2 layers) were deposited on the SL surface. GaAs substrates were removed by a highly-selective etch, so free-standing SL films of 1–2 mm diameter were prepared.

The Raman spectra were measured at temperatures of 80 and 300 K using triple Dilor XY spectrometer equipped with multichannel CCD detector and Jobin Yvon U1000 double spectrometer with GaAs photomuliplier. Raman scattering was excited below the SL bandgap using the 647.1 and 676.4 nm lines of a Kr^+ laser (their energies are 1.92 and 1.83 eV). The laser plasma lines (236 and 229 cm^{-1} for excitation lines of 647.1 and 676.4 nm, respectively) were used as references to ensure the high accuracy in the measurements of phonon frequencies. The forward and backscattering spectra were measured at the same point of sample surface (fixed with respect to the collecting lens) under the same excitation power densities, so any phonon frequency shifts due to sample inhomogeneity or heating were excluded.

3 Results and discussion

Figure 1 plots the Raman spectra of the sample A in three geometries schematically shown in the inset: (a) backscattering from the (001) surface under normal incidence ($\Theta = 0$); (b) back-scattering under the Brewster-angle-incidence (75° from the normal to SL surface, internal angle $\Theta = 16°$); and (c) forward scattering ($\Theta = 90°$). Backscattering spectra are typical for (001)-grown SL's [1–3]. They contain peaks of odd-order confined LO phonons in $z(x,y)\bar{z}$ polarization configuration, and even modes (LO_2) are dominant in parallel $z(x,x)\bar{z}$ geometry. However, the LO_1 line is slightly shifted towards lower frequencies as the phonon wavevector acquires in-plane component (spectra b), while the LO_2 peak position remains unchanged. In the forward scattering spectra the frequency positions of LO_1 and LO_2 lines almost coincide. There is also a slight shift of LO_3 line as compared to backscattering spectra. In the sample A this behaviour is more pronounced for GaAs phonons. In the AlAs region the forward scattering spectra are not so clear but the phonon lines reveal similar evolution as the scattering geometry is changed. In the sample B having lower layer thicknesses the frequency shifts of odd-order AlAs phonons are more noticeable (Fig. 2). The room-temperature spectra have the same shape as those for $T = 80$ K, the phonon lines are only homogeneously

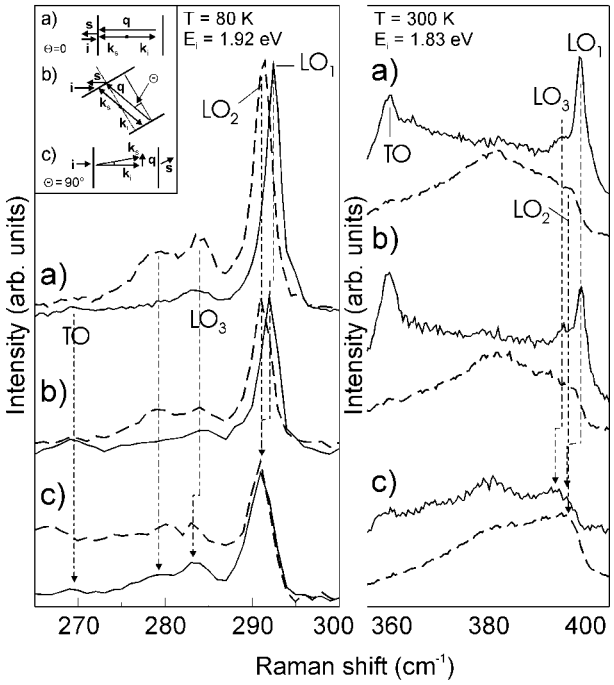

Fig. 1. Raman spectra of sample A in three different scattering geometries schematically shown in the inset. Left and right panels show GaAs and AlAs regions, respectively. Solid and dashed lines correspond to crossed (x,y) and parallel (x,x) polarization configurations. Dashed-dotted lines are guides to eye.

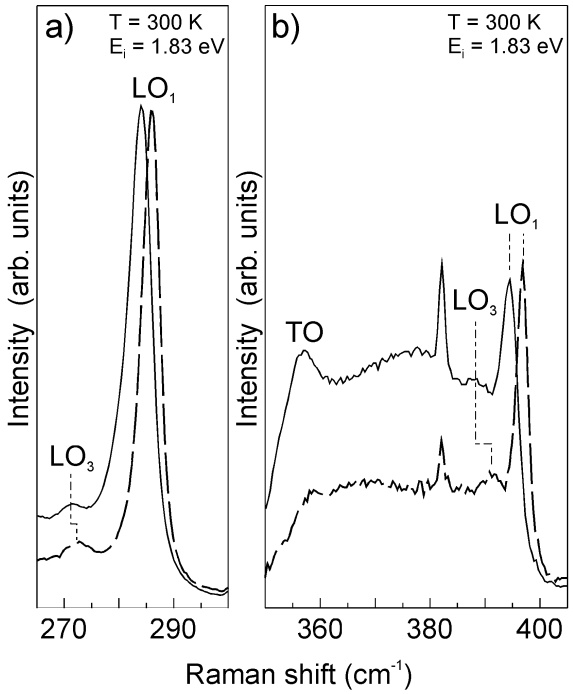

Fig. 2. Raman spectra of sample B (crossed polarizations) in backscattering (dashed line) and forward scattering (solid line) for GaAs (a) and AlAs (b) optical phonon regions. The sharp peak at 382 cm^{-1} is a Kr^+ laser plasma line.

shifted towards lower frequencies (by about 3.5 cm^{-1}) and broadened.

To explain our experimental data we have calculated the angular dispersion for GaAs/AlAs SL's using the dielectric susceptibility model for optical phonons in SL's by Dumelow and Smith [8]. In this model the properties of superlattice long-wavelength optical vibrations are considered from the point of view of the anisotropic dielectric function. In our Raman experiments the maximum absolute wavevector value is $|\mathbf{q}| = 6.6 \times 10^5\,\mathrm{cm}^{-1}$ (for backscattering). For such a small wavenumbers the calculated angular dispersions are practically independent on $|\mathbf{q}|$. The $|\mathbf{q}|$-dependence becomes significant at larger wavenumbers [7] (about 10^7 cm^{-1}). So, in our case we can use the long-wavelength limit $|\mathbf{q}| \to 0$. An (001)-grown SL can be considered as a uniaxial medium, and the dielectric tensor ε is represented by its principal components $\varepsilon_{xx} = \varepsilon_{yy}$ and ε_{zz}. In short-period superlattices, the effects of phonon confinement in the z-direction must be taken into account, so the general form of the dielectric tensor (ignoring damping) is [8]:

$$\varepsilon_{xx} = \varepsilon_{xx}^{\infty}\left[1 + \sum_j \frac{S_{Tj}}{(\omega_{Tj}^2 - \omega^2)}\right],$$
$$\frac{1}{\varepsilon_{zz}} = \frac{1}{\varepsilon_{zz}^{\infty}}\left[1 - \sum_j \frac{S_{Lj}}{(\omega_{Lj}^2 - \omega^2)}\right], \qquad (1)$$

where ω_{Lj} and ω_{Tj} are the frequencies of the confined LO and TO modes of index j, S_{Lj} and S_{Tj} are their oscillator strengths. The summation over j covers all confined phonon modes of both SL constituents. $\varepsilon_{xx}^{\infty}$ and $\varepsilon_{zz}^{\infty}$ are the principal components of the high-frequency dielectric tensor given by

$$\varepsilon_{xx}^{\infty} = \frac{d_1\varepsilon_1^{\infty} + d_2\varepsilon_2^{\infty}}{d_1 + d_2},$$
$$\frac{1}{\varepsilon_{zz}^{\infty}} = \frac{d_1(\varepsilon_1^{\infty})^{-1} + d_2(\varepsilon_2^{\infty})^{-1}}{d_1 + d_2}, \qquad (2)$$

where d_1 and d_2 are the thicknesses of the constituent layers, ε_1^{∞} and ε_2^{∞} are their bulk high-frequency dielectric constants.

The propagation of electromagnetic wave in a medium having the dielectric function (1) is described by standard expressions [8]. For p-polarized (in the xz-plane) modes the propagation equation is

$$\frac{q_x^2}{\varepsilon_{zz}} + \frac{q_z^2}{\varepsilon_{xx}} = \frac{\omega^2}{c^2}\,. \qquad (3)$$

We consider propagation in the xz-plane with the angle Θ between $\mathbf{q}$ and z-axis, so $\tan\Theta = q_x/q_z$. In the unretarded limit $c \to \infty$ (3) becomes

$$\tan^2\Theta = -\frac{\varepsilon_{zz}}{\varepsilon_{xx}}\,. \qquad (4)$$

For s-polarization (normal to the xz-plane) the unretarded limit yields $\varepsilon_{xx}^{-1} = 0$, so the s-polarized TO phonons have no angular dispersion. Equation (4) describes the angular dispersion of long-wavelength p-polarized phonons in SL's. It can be used in combination with any superlattice model that yields a dielectric function, either continuum or microscopic [8]. In the present work we used the microscopic linear chain model including nearest and next-nearest neighbour interactions [16]. This model gives the superlattice dielectric function in the form (1) using the effective ionic charges obtained from bulk LO-TO splittings of SL constituents.

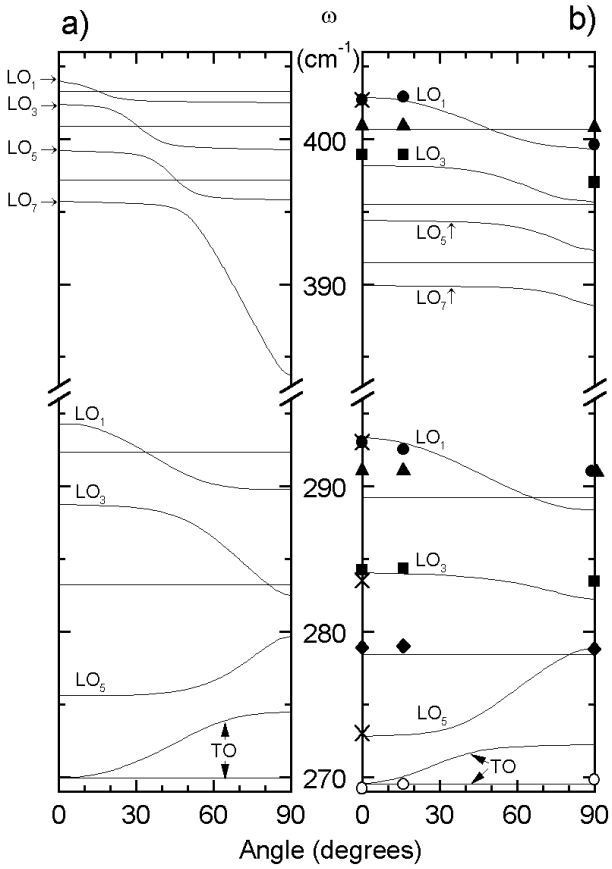

Fig. 3. Angular dispersion of optical phonons calculated with dielectric susceptibility model of reference [8]. (a) Ideal $(GaAs)_7(AlAs)_7$ superlattice; (b) $(GaAs)_8(AlAs)_7$ superlattice with interface broadening parameter $W = 1.7$. Symbols plot experimental mode frequencies: LO_1 (solid circles), LO_2 (triangles), LO_3 (squares), LO_4 (diamonds), and TO_1 (open circles). Crosses indicate the phonon frequencies measured in backscattering on the sample A before removing substrate.

Figure 3a shows the angular dependence of optical phonon frequencies for ideal $(GaAs)_7(AlAs)_7$ SL in the long-wavelength limit. Similar results have been obtained using other models [4–7]. As one can see, the calculation predicts significant decrease of the highest-order odd LO mode frequencies (LO_1 and LO_3) as the angle Θ between the phonon wavevector and SL axis increases from 0 to 90°, whereas the even-order modes are dispersionless. When the frequency of LO_1 mode approaches that of the mode with the same symmetry (LO_3),

these modes mix (anticross). Interaction does not occur with the even modes having opposite symmetry. It should be noted that classification of modes in terms of mode number and polarization becomes meaningless for $\Theta \neq 0$ because of mode mixing. Nevertheless, for identification purposes we label modes by their numbers at $\Theta = 0$.

At $\Theta = 90°$ the calculation for ideal SL (Fig. 3a) yields that the highest-energy mode is LO_2, and the position of LO_1 line is close to that of LO_3 at $\Theta = 0$. However, the experimentally observed LO_1 mode frequency is significantly higher (it is very close to the LO_2 line). Also, the observed LO_3 mode angular shift is much smaller than the calculation predicts. We believe the disagreement is due to the influence of interface disorder that is always present in any real SL structure. The interface broadening effects on confined (having zero in-plane wavevector component) optical phonons have been studied by a number of authors [14–17]. As disorder causes changes in $\Theta = 0$ optical mode frequencies and dielectric tensor components, it should also influence the phonon angular dispersion. The dielectric susceptibility model enables to include the interface roughness effects [8,16] as it only needs the frequencies and atomic displacements for LO and TO phonons propagating along the SL growth direction. The $\Theta = 0$ mode frequencies and displacements can be calculated within any model taking into account interface roughness. We used the above mentioned linear chain model of Samson *et al.* [16], in which an interface broadening is included by considering SL cationic layers as a mixture of Ga and Al atoms. Each cationic site is described by two equations of motion for Ga and Al atoms with weight factors P_{Ga} and P_{Al}. These are the probabilities of occupation of the site by Ga (Al) atoms. ($P_{\mathrm{Ga}} + P_{\mathrm{Al}} = 1$). The error function is used to describe interface broadening, so the probability of occupation of a cationic site at the distance z from AlAs/GaAs interface by Ga atoms is given by

$$P_{\mathrm{Ga}}(z) = \frac{1}{2}\left[1 + \mathrm{erf}\left(\frac{z}{W}\right)\right], \qquad (5)$$

where W is the interface broadening parameter.

For the determination of actual sample parameters we have measured Raman backscattering spectra of folded acoustic and confined optical phonons before removing substrate. To exclude the contribution of substrate phonons to the spectra we used the 514.5 nm of Ar^+ laser for excitation. This line is effectively absorbed by the 100-period SL, so there is no signal from the substrate. These spectra for sample A are shown in Figure 4. From the data of the 1st folded LA doublet and confined GaAs optical modes LO_1, LO_3, LO_5 we have determined the following parameters (the procedure is described in Ref. [17]): total period $d = 15$, thicknesses of GaAs and AlAs layers $d_1 = 8$, $d_2 = 7$; the interface broadening parameter $W = 1.7$ (all the parameters are given in monolayer units; 1 monolayer = 0.283 nm).

Figure 3b plots the angular dispersion for GaAs/AlAs SL calculated with the actual parameters of layer thicknesses and interface intermixing given above. Experimental data are shown by symbols. As one can see, interface roughness leads to significant changes both in $\Theta = 0$ phonon frequencies and their angular dependence. Agreement between calculated dispersion and experimental data is quite good. The model gives a somewhat higher GaAs $LO_1 - LO_2$ difference for $\Theta = 0$ than that measured in the experiment. This is likely due to the flatness of the bulk GaAs LO phonon dispersion curve at small wavevector values ($q \leq 0.2\pi/a_0$, where a_0 is the lattice constant) [18,19], a fact that was not taken into account in our calculations.

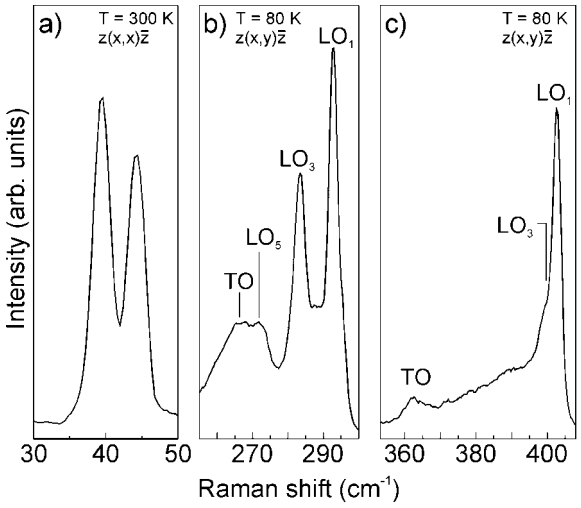

Fig. 4. Raman spectra of sample A with unetched substrate ($E_i = 2.41$ eV) used for sample characterization. (a) 1st folded LA doublet, (b) and (c) GaAs and AlAs optical phonon regions, respectively.

It should be noted that the optical phonon anisotropy has been observed in Raman spectra only under excitation in the transparency range, *i.e.* away from resonance below the SL bandgap. We have also studied SL's with thicker GaAs layers $(GaAs)_9$ $(AlAs)_9$ and $(GaAs)_9$ $(AlAs)_5$ (samples C and D). For these SL's the excitation conditions are resonant (the laser energies $E_i = 1.92$ eV and $E_i = 1.83$ eV, are close to the SL excitonic transitions at $T = 80$ and 300 K, respectively). In this case both forward and backscattering spectra (Fig. 5) contain peaks of GaAs highest-order even confined optical phonon LO_2 and interface phonon features IF_1 and IF_2 in GaAs and AlAs regions. We did not observe any notable shifts of the phonon lines in resonant spectra when the geometry is changed from back- to forward scattering. This fact is explained by the breakdown of momentum conservation in its simplest form. The relation $\mathbf{k}_{\mathrm{s}} = \mathbf{k}_{\mathrm{i}} \pm \mathbf{q}$ (where $\mathbf{k}_{\mathrm{i}}$ and $\mathbf{k}_{\mathrm{s}}$ are wavevectors of incident and scattered light) is no longer true for the resonant process. It was shown in several works [20–22], that the dominant mechanism of resonant Raman scattering by optical phonons in superlattices is defect-induced Fröhlich interaction. This process includes, as well as scattering by a phonon, an additional elastic scattering of excitons by impurities or interface roughness. Therefore, phonons with non-zero in-plane wavevector components q_x can be involved in the Raman process in both forward and backscattering geometries.

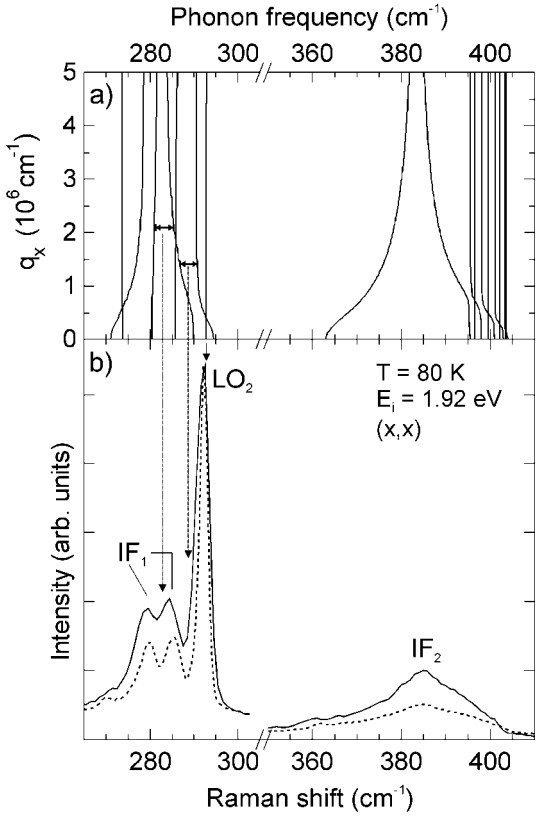

Fig. 5. (a) Dependence of optical phonon frequencies on in-plane wavevector q_x for $(GaAs)_9(AlAs)_9$ SL, calculated for fixed q_z component 6.6×10^5 cm^{-1}. (b) Resonant Raman spectra of $(GaAs)_9(AlAs)_9$ SL in forward (solid line) and backscattering (dashed) geometries. Spectra are normalized to the GaAs LO_2 intensity.

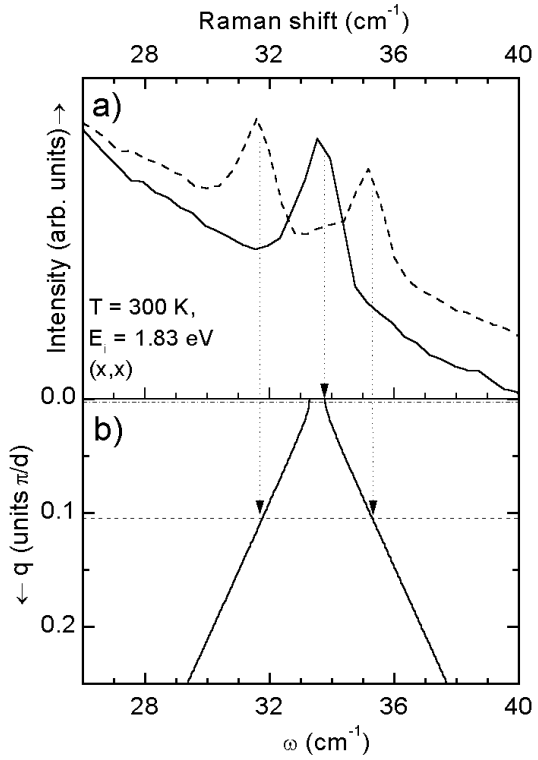

Fig. 6. (a) Resonant Raman spectra of sample C in acoustic region (parallel polarization configuration). Solid and dashed lines correspond to forward and backscattering geometries. (b) Part of folded LA phonon dispersion curve for $(GaAs)_9(AlAs)_9$ superlattice. Horizontal lines indicate the value of wavevector transfer in backscattering (dashed line) and forward scattering (dashed-dotted) for laser energy $E_i = 1.83$ eV.

The features below the GaAs LO_2 peak in resonant Raman spectra of SL's were firstly attributed to higher-order even confined modes (LO_4, LO_6 *etc.*) [1,3]. More recently Shields *et al.* [23,24] offered another interpretation of these lines as broad features of so-called interface phonons (IF). These are vibrations evolving out of the highest-order odd confined LO and TO modes as the in-plane wavevector increases [4–6,11]. Since the phonons with a range of in-plane wavevectors can participate in defect-induced resonant Raman process, spectra reveal broad feature between the LO_1 and TO_1 mode frequencies. In the GaAs region this broad line has several minima due to anticrossings between the odd-order confined modes having the same symmetry [23,24]. This is illustrated in Figure 5a showing the q_x dependence of optical phonon frequencies in $(GaAs)_9(AlAs)_9$ SL, calculated with the modified continuum model of Chamberlain *et al.* [7] for the fixed z-component of phonon wavevector ($q_z = 6.6 \times 10^5$ cm^{-1}, as for backscattering). In the AlAs region the minima due to anticrossings are narrow and not resolved in the experiment.

The only difference observed between forward and backscattering resonant Raman spectra of samples C and D is the intensity ratio of LO_2/IF lines. It is larger (by a factor of 1.6–1.9) for forward scattering. This can be explained if these features are attributed to interface phonons. In backscattering the modes with $q_x \neq 0$ are present only due to the above mentioned higher-order process involving scattering by defects. In forward scattering this mechanism also takes place, but in this case the phonons with non-zero component q_x can participate as well in the simple phonon-only Raman process. So, the interface phonon features are additionally enhanced in forward Raman spectra.

We note that the defect-induced mechanism that causes the breakdown of wavevector conservation is dominant only for resonant Raman scattering by optical phonons. In the acoustic phonon region the relation $\mathbf{k}_s = \mathbf{k}_i \pm \mathbf{q}$ remains valid in the resonant Raman process, and we observed a clear difference between back- and forward scattering spectra. Figure 6a plots the spectra of sample C in the region of the 1st folded LA doublet. The picture is quite similar to that firstly reported by Jusserand *et al.* [25] for off-resonance excitation. While in backscattering both lines of LA doublet are seen, only one line is observed in forward geometry. It is attributed to the A_1 component of the zone-centre doublet. The other (B_2) component is symmetry forbidden [1,25]. The single line in the forward scattering spectrum lies almost in the middle of

backscattering doublet due to very small value of the zone-centre gap in the LA dispersion for this SL (See Fig. 6b showing the 1st doublet area of the dispersion curve calculated using the elastic continuum model).

4 Conclusion

We have presented the results of Raman experiments in short-period GaAs/AlAs superlattices in three geometries: (a) backscattering normal to the sample surface, (b) backscattering at oblique incidence, and (c) forward scattering. These experiments allow to observe the zone-centre optical phonon anisotropy in superlattices. We have compared our experimental results with angular dispersion of optical phonons in superlattices calculated using dielectric susceptibility model. In our calculations we considered both ideal superlattices and real structures with actual parameters of layer thicknesses and interface intermixing. The agreement is much better if the interface roughness is taken into account.

The resonant Raman spectra of superlattices reveal only changes in the relative intensity of phonon lines as the scattering geometry is turned from back- to forward scattering while the frequency positions do not shift. This behaviour is explained in the frame of recently developed theory of resonant Raman line shapes of optical phonons in superlattices.

We would like to thank Dr. A.G. Milekhin for help and useful discussions. This work was supported in part by the Russian Basic Research Foundation (Grant No. 98-02-17827). D.A.T. thanks the Sächsischen Ministerium für Wissenschaft und Kunst for financial support, and the Semiconductor Physics group of the TU Chemnitz for hospitality.

References

1. B. Jusserand, M. Cardona, in *Light Scattering in Solids V*, edited by M. Cardona, G. Güntherodt (Springer, Berlin, 1989), p. 49.
2. T. Ruf, *Phonon Raman scattering in semiconductors, quantum wells and superlattices* (Springer, Berlin, 1998).
3. A.K. Sood, J. Menendez, M. Cardona, K. Ploog, Phys. Rev. Lett. **54**, 2111 (1985).
4. E. Richter, D. Strauch, Solid State Commun. **64**, 867 (1987).
5. S.F. Ren, H.Y. Chu, Y.-C. Chang, Phys. Rev. B **40**, 3060 (1989).
6. H. Rücker, E. Molinari, P. Lugli, Phys. Rev. B **45**, 6747 (1992).
7. M.P. Chamberlain, M. Cardona, B.K. Ridley, Phys. Rev. B **48**, 14356 (1992).
8. T. Dumelow, S.R.P. Smith Phys. Rev. B **57**, 3978 (1998). See also T. Dumelow, T.J. Parker, S.P.R. Smith, D.R. Tilley, Surf. Sci. Rep. **17**, 151 (1993).
9. V.A. Haisler, D.A. Tenne, N.T. Moshegov, A.I. Toropov, I.I. Marakhovka, A.P. Shebanin, JETP Lett. **61**, 376 (1995).
10. R. Hessmer, A. Huber, T. Egeler, M. Haines, G. Tronkle, G. Weimann, G. Abstreiter, Phys. Rev. B **46**, 4071 (1992).
11. G. Scamarcio, M. Haines, G. Abstreiter, E. Molinari, S. Baroni, A. Fischer, K. Ploog, Phys. Rev. B **47**, 1483 (1993).
12. M. Zunke, R. Schörer, G. Abstreiter, W. Klein, G. Weimann, M.P. Chamberlain, Solid State Commun. **93**, 847 (1995).
13. A. Fainstein, P. Etchegoin, M.P. Chamberlain, M. Cardona, K. Tötemeyer, K. Eberl, Phys. Rev. B **51**, 14448 (1995).
14. B. Jusserand, F. Alexandre, D. Paquet, G. Le Roux, Appl. Phys. Lett. **47**, 301 (1985).
15. E. Molinari, S. Baroni, P. Giannozzi, S. de Gironcoli, Phys. Rev. B **45**, 4280 (1992).
16. B. Samson, T. Dumelow, A.A. Hamilton, T.J. Parker, S.P.R. Smith, D.R. Tilley, C.T. Foxon, D. Hilton, K.J. Moore, Phys. Rev. B **46**, 2375 (1992).
17. V.A. Haisler D.A. Tenne, N.T. Moshegov, A.I. Toropov, A.P. Shebanin, A.A. Yaskin, Physics of the Solid State, **38**, 1235 (1996).
18. S. Baroni, P. Giannozzi, E. Molinari, Phys. Rev. B **41**, 3870 (1990).
19. D. Strauch, B. Dorner, J. Phys.-Cond. **2**, 1457 (1990).
20. W. Kauschke, A.K. Sood, M. Cardona, K. Ploog, Phys. Rev. B, **36**, 1612 (1987).
21. A. Alexandrou, M. Cardona, K. Ploog, Phys. Rev. B **38**, 2196 (1988).
22. A.J. Shields, C. Trallero-Giner, M. Cardona, H.T. Grahn, K. Ploog, V.A. Haisler, D.A. Tenne, N.T. Moshegov, A.I. Toropov, Phys. Rev. B **46**, 6990.
23. A.J. Shields, M. Cardona, K. Eberl, Phys. Rev. Lett. **72**, 412 (1994).
24. A.J. Shields, M.P. Chamberlain, M. Cardona, K. Eberl, Phys. Rev. B, **51**, 17728 (1995).
25. B. Jusserand, F. Alexandre, J. Dubard, D. Paquet, Phys. Rev. B **33**, 2897 (1986).